

Combining optical spectroscopy and interferometry

Stefan Kraus¹

University of Exeter, Astrophysics Group, Physics Building, Stocker Road, Exeter, EX4 4QL, UK

Received September 2, 2013, accepted November 5, 2013

Key words methods: observational, techniques: interferometric, spectroscopic, stars: emission-line, formation, kinematics

Modern optical spectrographs and optical interferometers push the limits in the spectral and spatial regime, providing important new tools for the exploration of the universe. In this contribution I outline the complementary nature of spectroscopic & interferometric observations and discuss different strategies for combining such data. Most remarkable, the latest generation of “spectro-interferometric” instruments combine the milliarcsecond angular resolution achievable with interferometry with spectral capabilities, enabling direct constraints on the distribution, density, kinematics, and ionization structure of the gas component in protoplanetary disks. I will present some selected studies from the field of star- & planet formation and hot star research in order to illustrate these fundamentally new observational opportunities.

©

1 Introduction

Since more than a century, spectroscopy is one of the most fundamental and universal tools in observational astronomy. With their ever-increasing sensitivity, spectral resolution, and calibration accuracy, the latest generation of optical spectrographs enables new applications, both in galactic and extragalactic astronomy. For instance, in the field of star- and planet formation, spectroscopic and spectrophotometric observations are indispensable to characterize the dust emission in protoplanetary disks (with low spectral resolution, but wide wavelength coverage), or to determine the accretion and mass-loss processes in these objects (with high spectral resolution observations in diagnostic lines).

For many applications, the main challenge in the interpretation of spectral line observations is the lack of information about the spatial distribution of the line-emitting gas. This lack of spatial information is typically compensated by introducing model assumptions, which allow us to relate a certain physical scenario with the measured spectrum. Unfortunately, these models often include a large number of free parameters, which can result in *parameter degeneracies*, where different parameter combinations result in similar spectra. Another problem are *model degeneracies*, where different classes of physical models can not be distinguished using spectroscopic data. In some cases, these model classes might correspond to fundamentally different physical scenarios. For instance, in the case of the Herbig Ae/Be stars, it is still debated whether the Br γ emission in these objects traces mass accretion or mass outflow processes (see discussion in Kraus et al., 2008). These degeneracies become more and more severe, as the models become more and more complex.

Fortunately, many of the aforementioned limitations and degeneracies can now be solved using optical interferom-

eters such as ESO’s Very Large Telescope Interferometer (VLTI), which combine the light from separate optical apertures in order to reach an unprecedented, milliarcsecond (mas) angular resolution. In this contribution, I would like to outline how spatially and spectrally resolved observations can be combined in order to solve some of the aforementioned model ambiguities, where I consider three approaches: In Section 2, I discuss some of the opportunities provided by coordinated spectroscopic and interferometric observations, while Section 3 discusses the ultimate combination of these techniques in *spectro-interferometry*. Another interesting and resources-efficient approach for obtaining some gas kinematical constraints is *spectro-astrometry*, which I will discuss in Section 4.

2 Complementary constraints from spectroscopy & interferometry

In order to illustrate the complementary nature of spectroscopy and interferometry, I discuss below our recent project on the pre-transitional disk of V1247 Orionis (Kraus et al., 2013), where we combined VLTI+Keck+Gemini infrared interferometry with IRTF, Spitzer, and HARPS spectroscopy.

V1247 Ori is a F0-type star located in the Orion OB1 b association. Earlier photometric observations on V1247 Ori measured a strong near- and far-infrared excess, but a deficit at mid-infrared wavelengths (Caballero, 2010), compared to classical T Tauri or Herbig Ae/Be disks. Given the coarse sampling of these earlier photometric observations, we obtained new spectroscopic observations using the near-infrared IRTF/SpeX (0.8-5.4 μm) and mid-infrared IRTF/BASS (2.9-13.5 μm) spectrograph, and complement them with archival Spitzer/IRS (5.2-38 μm) and HARPS

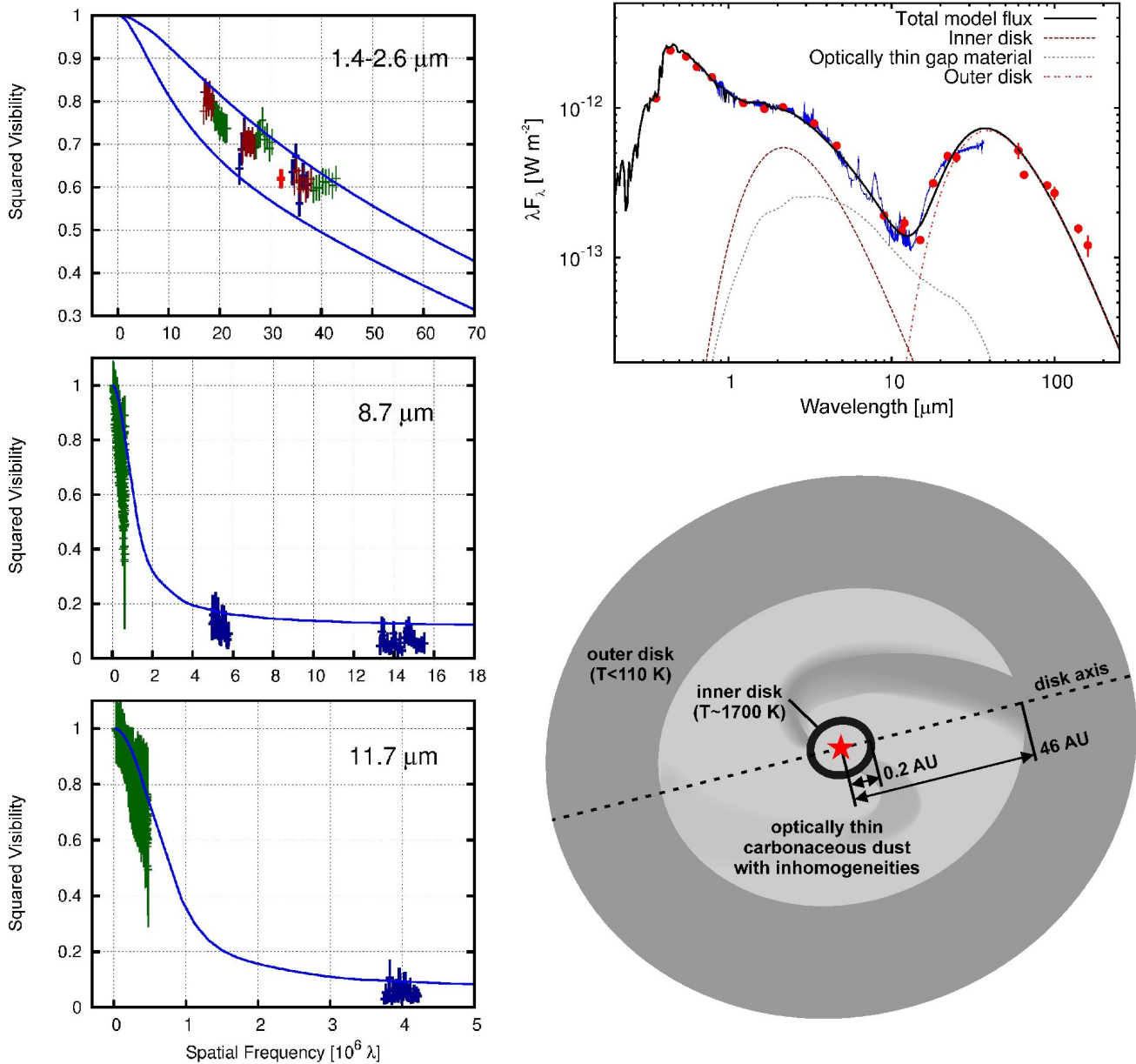


Fig. 1 We use our multi-wavelength visibilities (left) and spectral energy distribution (top right) to constrain the global geometry of the pre-transitional disk V1247 Orionis. The sketch in the bottom right illustrates our best-fit model, which includes an extended gap that separates the optically thick dust at the dust sublimation radius from the outer disk at $\gtrsim 46$ AU (Kraus et al., 2013).

(V-band) observations. The resulting spectral energy distribution (SED, Fig. 1, top right) clearly shows that V1247 Ori belongs to the class of “pre-transitional disks”, which are believed to exhibit extended disk gaps that might have been cleared by young planets located in the gap region (Espaillat et al., 2010). However, pure SED studies face serious ambiguities in solving the structure of these disks, as not only the radial structure of these disks, but also the viewing geometry and dust composition is unknown. Interferometry allows us to solve many of these ambiguities and to determine the location of the emitting material directly. For this purpose, we conducted near-infrared interferometric observations using

the VLTI/AMBER and Keck Interferometer/V2-SPR instrument (*H* and *K*-band), as well as mid-infrared interferometry using the VLTI/MIDI instrument (*N*-band). These long-baseline interferometric observations cover baseline lengths between 43 and 125 m and were complemented with Gemini/TreCS speckle interferometry and Keck/NIRC2 aperture masking interferometry, which sample shorter baseline lengths < 8 m.

In order to model the interferometric data we require knowledge about the stellar properties. Unfortunately, the spectral type classification in the literature shows a wide spread from F0V to A5III. Therefore, we repeated the clas-

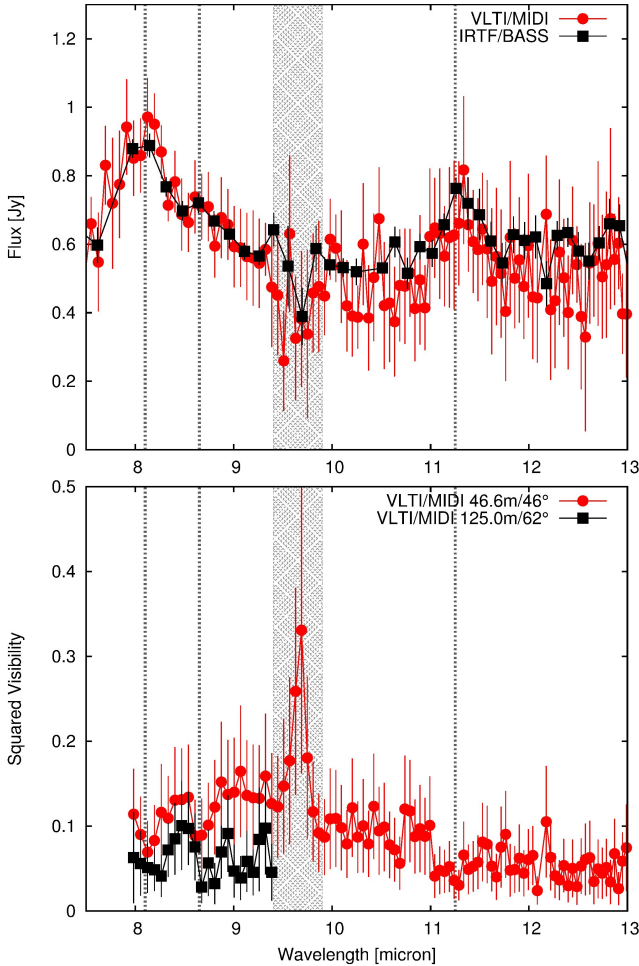


Fig. 2 Spectrally dispersed mid-infrared visibilities measured on V1247 Ori. The measurements in the gray shaded area are affected by an atmospheric Ozone absorption feature. Within the hydrocarbon (PAH) features (dashed lines), we detect a clear drop in visibility, indicating that these compounds are located at larger stellocentric radii than the continuum-emitting dust species.

sification using the HARPS spectra and find best agreement with spectral type F0V ($T_{\text{eff}} = 7250$ K), where we adopt a distance of 385 ± 15 pc for the Alnilam cluster (Caballero & Solano, 2008).

Using our mid-infrared interferometric observations, we determined the disk inclination angle to $31.3 \pm 7.5^\circ$. We then model the interferometric visibilities and SED data using a temperature power-law disk model (Fig. 1). The near-infrared emission traces a ring-like inner disk that is located at the dust sublimation radius at 0.2 AU. This narrow inner disk is separated from the outer disk that starts at 46 AU. Surprisingly, we find that the gap region is filled with significant amounts of optically thin material with a carbon-dominated dust mineralogy. State-of-the-art SED models often associate this MIR excess emission to a heated wall of the outer disk (e.g. Espaillat et al., 2011), which illustrates the importance of our multi-wavelength interferome-

try approach for unveiling the real geometry of these important objects.

Besides the dust continuum, our spectrally dispersed VLT/MIDI N -band observations also cover spectral features corresponding to the hydrocarbon (PAH) emission (Fig. 2, top). The measured visibilities show a small drop of visibility at the position of the PAH lines (Fig. 2, bottom), which indicates that the PAH-emission originates from significantly larger stellocentric radii than the dust continuum, likely the outer disk.

Finally, our Keck/NIRC2 aperture masking interferometry (H , K' , and L band) reveals non-zero phase signals, which indicate asymmetries in the brightness distribution on scales of 10..20 AU, i.e. within the gap region. The detected asymmetries are highly significant, yet their amplitude and direction changes with wavelength, which is not consistent with a companion interpretation but indicates asymmetries in the disk structure itself. We interpret this as strong evidence for the presence of complex density structures, possibly reflecting the dynamical interaction of the disk material with sub-stellar mass bodies that are responsible for the gap clearing.

V1247 Ori exhibits photometric occultation events and spectroscopic variability (Caballero, 2010; Kraus et al., 2013), possibly indicating highly dynamic processes that might be at work in the inner disk regions. An important objective of future investigations will be to investigate the origin of this variability. Espaillat et al. (2011) monitored a sample of pre-transitional disks with Spitzer spectroscopy and found that the variability shows an anti-correlated behaviour at NIR and MIR wavelengths. In order to explain both the timescale and spectral behaviour of the variability, they proposed shadowing effects from co-rotating disk warps at the inner dust rim, probably triggered by orbiting planets. Such warps are also predicted by hydrodynamic simulations of disks with embedded planets (e.g. Fouchet et al., 2010) and would result in a highly asymmetric brightness distribution.

Multi-epoch interferometric imaging observations could allow us to detect these planet-induced disk structures and to trace their evolution and orbital motion around the star, which would provide new observational constraints on theories of disk dispersal and planet formation. These interferometric observations should be accompanied with extensive spectroscopic monitoring, which might enable to relate any detected structural changes with the observed spectro-/photometric variability.

3 Spectro-interferometry: Spectroscopy meets long-baseline interferometry

In the last chapter, I outlined the advantages of coordinating spectroscopic and interferometric observations in a joint observing campaign. Even more powerful constraints are provided by *spectro-interferometric* instruments that incor-

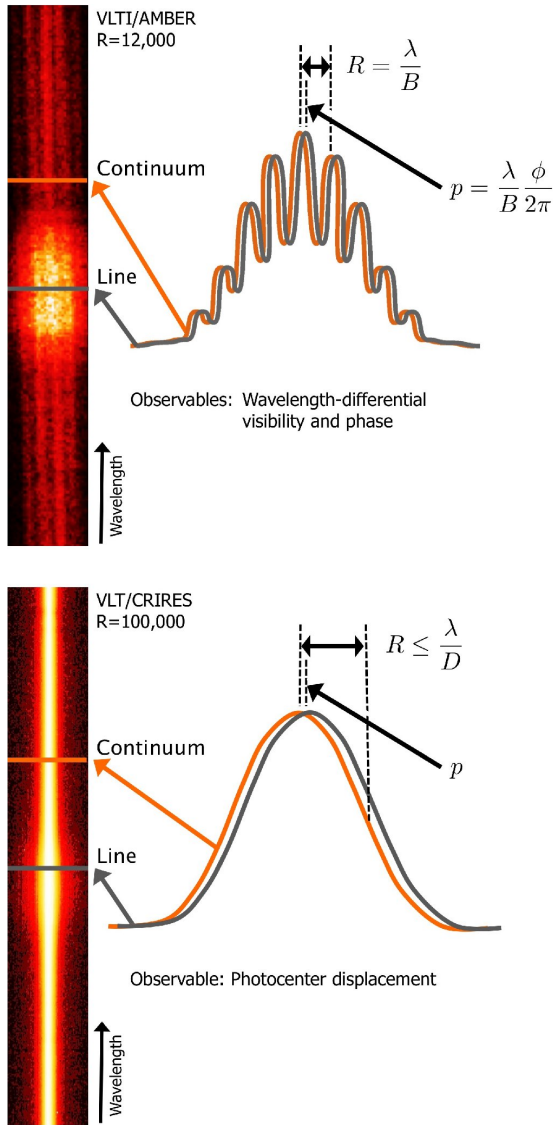


Fig. 3 *Top:* Spectro-interferometry uses spectrally dispersed interferograms (such as the VLT/AMBER $R = 12,000$ interferogram from Weigelt et al. 2007 shown here) in order to detect phase differences between the continuum emission and the emission within a spectral line. In first-order expansion, this differential phase ϕ correspond to the photocenter offset p between the continuum- and line-emitting region. *Bottom:* Spectro-astrometry computes the centroid position in conventional high-SNR spectra (such as the VLT/CRIRES spectrum from Kraus et al. 2012b shown here), and measures the minuscule photocenter differences in the centroid position between the continuum and line spectral channels.

porate high-resolution spectrographs in order to spectrally disperse the interferometric signals directly.

From these dispersed interferograms, we can derive the visibility amplitude (interferogram contrast) and phase (interferogram shift) in hundreds of spectral channels. The visibilities and phases allow us to constrain the brightness distribution in each of these spectral channels, covering simultaneously the continuum and emission or absorption lines. A particularly useful quantity is the differential phase (ϕ in Fig. 3, top), i.e. the phase difference between different spectral channels, which is also one of the few quantities that are invariant to atmospheric perturbations (Petrov, 1989). For marginally resolved objects, the differential phase in a certain spectral line channel is directly related to the photocenter displacement p of the line-emitting region with respect to the photocenter of the continuum emission, as projected on the telescope baseline. The typical differential phase accuracy that can currently be reached is $\sim 1^\circ$, which for a 100 m baseline corresponds to a photocenter displacement of just 0.012 mas or 0.002 AU ($= 0.5 R_\odot$) at the distance of the Taurus star forming region. Measurements towards at least two different position angles on the sky (which can be obtained from a single 3-telescope observations) are required in order to “triangulate” the 2-D photocenter vector \vec{p} from these baseline-projected photocenter offsets.

The two operational instruments that offer this observing mode with sufficient resolution for detailed kinematical studies are the near-infrared VLT/AMBER instrument (spectral resolution up to $\lambda/\Delta\lambda = 12\,000$, Petrov et al., 2007) and the visual wavelength VEGA instrument at the CHARA array (up to $\lambda/\Delta\lambda = 35\,000$, Mourard et al., 2012).

For instance, in a recent study we used AMBER in order to study the disks around classical Be stars (Kraus et al., 2012c). Classical Be stars are surrounded by a gaseous disk that is formed of ejected stellar material. However, both the ejection mechanism and the subsequent evolution of the disk material remain poorly understood. The proposed scenarios include radiatively driven winds, ram pressure or magnetically induced wind compression, and viscous decr-

tion (Porter & Rivinius, 2003). Our study on the classical Be star ζ Tau used AMBER’s medium resolution code ($R = 1500$) and covered the $\text{Br}\gamma$ $2.16\ \mu\text{m}$ and at least nine transitions from the Pfund series (Pf14-22, $2.359\text{--}2.448\ \mu\text{m}$). These lines can be covered with a single spectral setup in about one hour of total observing time, which makes these observations highly efficient. Both the Brackett and Pfund lines show a double-peaked profile (Fig. 4, top row), which is consistent with a disk rotation interpretation. In Figure 4 (bottom panels), we show the photocenter displacements that we have computed for ζ Tau, both for the $\text{Br}\gamma$ line (left panel), and the Pf14-22 lines (right panel). We find that the blue- and red-shifted line emission emerges from opposite directions with respect to the star, revealing the disk rotation axis (position angle $\sim 126^\circ$). The measured visibilities show a significant drop,

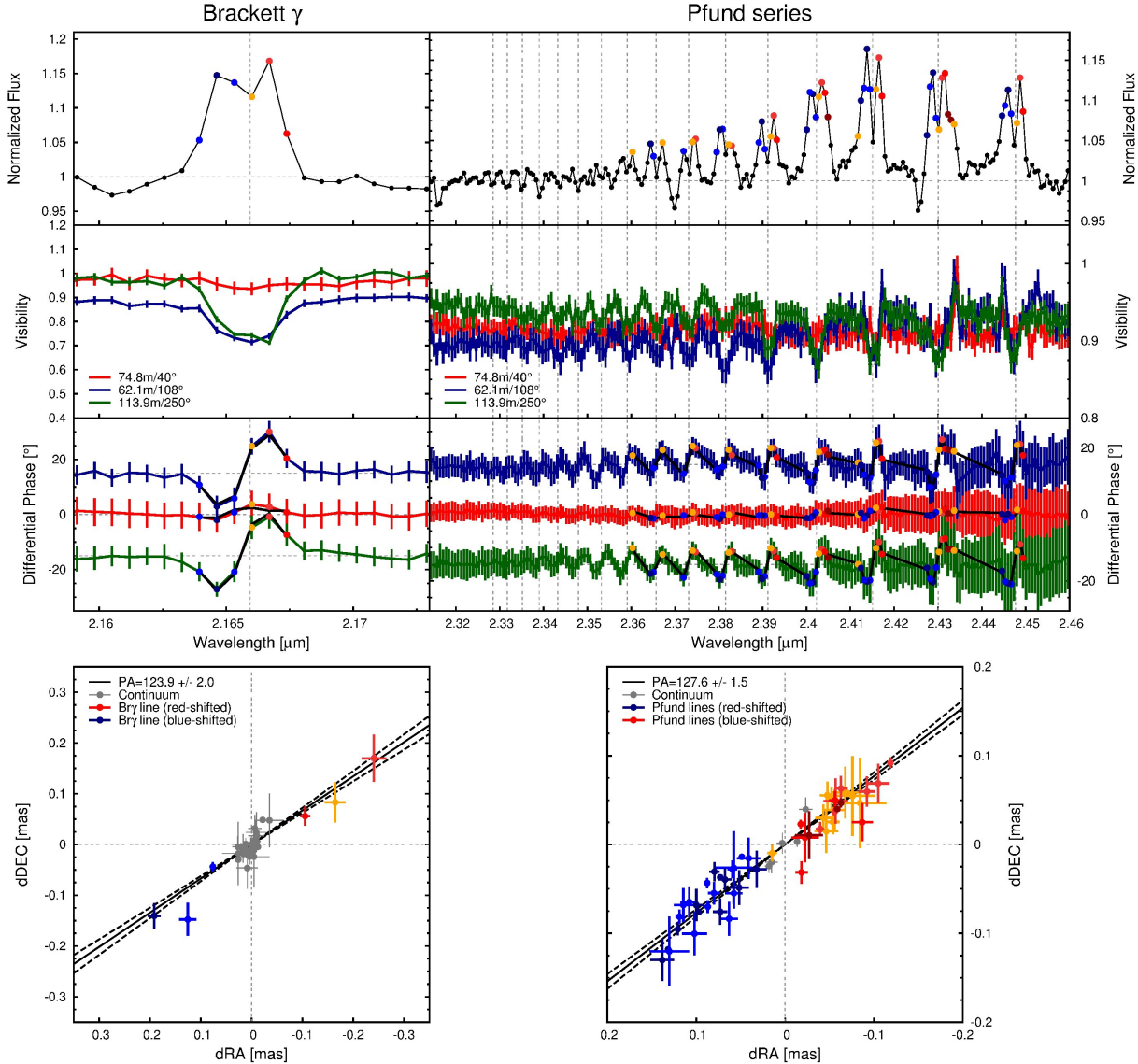


Fig. 4 VLT/AMBER spectro-interferometric data recorded on the classical Be star ζ Tau (Kraus et al., 2012c), including spectra (top row), visibility amplitudes (2nd row from top), and differential phases (3rd row). A single spectral setup covers the Br γ -line (left), as well as several line transitions from the Pfund series (right), where each line profile is clearly double-peaked. We derived the photocenter displacement vector (bottom panels), which shows that the blue- and red-shifted emission originates from opposite directions of the stellar continuum emission, revealing the disk rotation axis.

which indicates that the line emission originates from larger stellocentric radii than the underlying continuum emission.

We supplement our data with archival measurements for the H α line (Quirrenbach et al., 1994; Tycner et al., 2004; Vakili et al., 1998) and find that the Br γ -line originates from similar stellocentric radii as the H α -line, while the Pfund lines originate much closer to the star. Using a simple LTE model, we can reproduce the differences in the spatial origin of the line transitions and constrain the temperature and excitation structure of the disk (Fig. 5). More detailed observations should enable us to derive also the disk ionization and vertical temperature structure, which are currently difficult to access.

Further improvements in the efficiency of uv-sampling will also soon enable the reconstruction of interferometric images for each velocity channel, providing the equivalent to the “channel maps” in radio interferometry. First attempts in this direction have been presented for instance by Schmitt et al. (2009) and Millour et al. (2011).

4 Spectro-astrometry

Another technique that can provide detailed kinematical and spatial information about the gas distribution on AU-scales is spectro-astrometry. Spectro-astrometry uses high-SNR long-slit spectra to measure the centroid position of

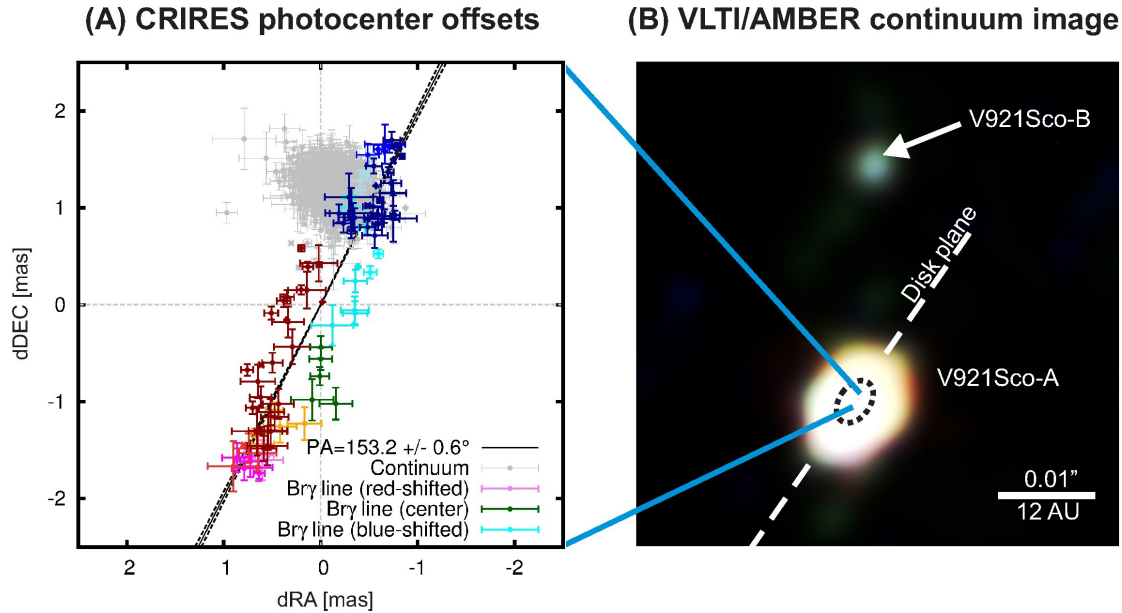


Fig. 6 *Left*: Photocenter displacement vectors derived from our VLT/CRIRES spectra on V921 Sco (Kraus et al., 2012b). *Right*: Color-composite of model-independent interferometric images (Kraus et al., 2012a) reconstructed from our low-spectral dispersion AMBER data on V921 Sco (blue: $1.65 \mu\text{m}$, green: $2.0 \mu\text{m}$, red: $2.3 \mu\text{m}$). The images have an effective resolution $\lambda/2B = 1.2 \text{ mas}$ and reveal a previously unknown companion at a separation of 24.9 mas (corresponding to 29 AU at 1.15 kpc).

an apparently unresolved object as function of wavelength (Fig. 3, bottom). By design, this technique is not able to resolve the line-emitting region directly (e.g. it does not provide visibility information), but it can reveal small-scale photocenter displacements, which are mathematically equivalent to the wavelength-differential phases measured in spectro-interferometry in the short-baseline regime. This makes it possible to combine the AMBER (visibility, differential phase, closure phase) and the spectro-astrometric signals directly for quantitative modeling, providing highly complementary constraints.

For our combined spectro-interferometry + spectro-astrometric observations, we employed the VLT/AMBER ($R = 12,000$) and VLT/CRIRES ($R = 100,000$) instruments and targeted the B[e] star V921 Scorpii (Kraus et al., 2012a,b). Important aspects about V921 Sco are still strongly debated, including its distance and evolutionary stage, where both a pre-main-sequence (e.g. Benedettini et al., 1998) and a post-main-sequence (e.g. Borges Fernandes et al., 2007) nature has been suggested.

The CRIRES spectra were obtained with the slit oriented towards three position angles ($55, 115, 175^\circ$) and the corresponding anti-parallel positions ($235, 295, 355^\circ$). The spectro-astrometric signals were derived for each position angle separately and then the signals towards parallel and anti-parallel position angles were subtracted, which provides an efficient method for eliminating instrumental artefacts (Brannigan et al., 2006).

Considering the CRIRES spectro-astrometric measurements alone leads to puzzling results: The photocenter in

the red-shifted line channels (red data points in Fig. 6, left) shows a significant offset of $\sim 3 \text{ mas}$, while the blue-shifted channels (blue data points) do not show a significant displacement with respect to the continuum channels (grey data points). This behaviour is not consistent with the expected signature for a rotating circumstellar disk, where the photocenter of the blue and red-shifted line emission should be displaced with similar amplitude in opposite directions from the central star, but might guide us to the interpretation that the $\text{Br}\gamma$ emission is associated, for instance, with a one-sided jet instead of a rotation disk.

However, the puzzle was solved with a VLT/AMBER aperture synthesis image that we reconstructed from AMBER continuum data (H and K -band; Fig. 6, right). The image reveals a previously unknown companion that is located at a separation of $25.0 \pm 0.8 \text{ mas}$ ($\sim 29 \text{ AU}$) in northern direction ($\text{PA } 353.8 \pm 1.6^\circ$) from the disk-harboring B0V-type star. Therefore, the continuum photocenter is shifted systematically towards the direction of the companion, while the primary star is located to a good accuracy half-way between the blue- and red-shifted photocenter vectors, consistent with a disk scenario.

Taking the presence of the companion into account, we then engaged in a detailed modeling of the spectro-astrometric and the detected strong AMBER visibility and differential phase signals (Fig. 7, 2nd and 3rd row from top). For this purpose, we tested rotation disks with different velocity profiles and found reasonable agreement with a Keplerian disk, where most of the line-emitting gas is located inside of the dust sublimation radius that we constrain to

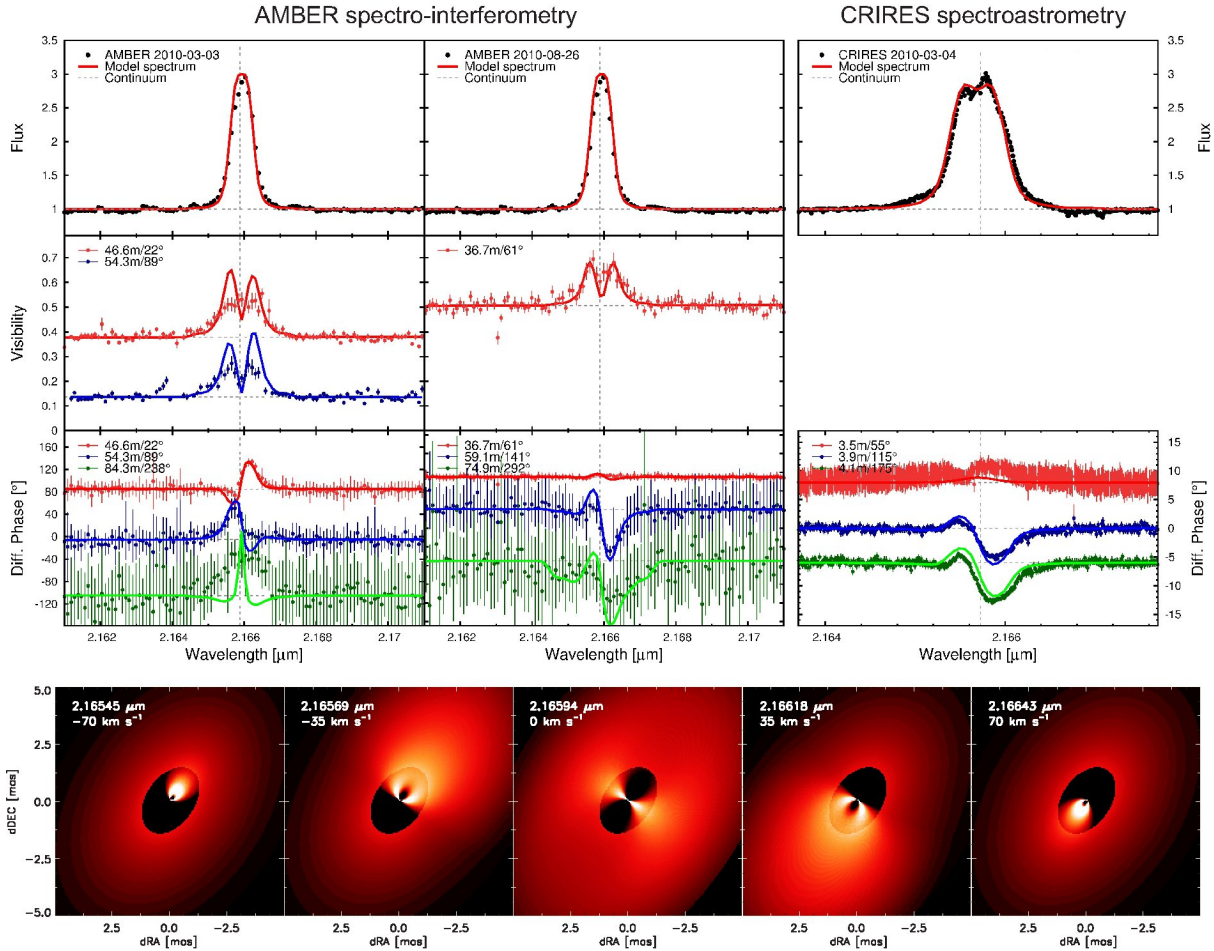


Fig. 7 *Top*: To constrain our V921 Sco model, we fitted the VLTI/AMBER spectra, visibilities, and differential phases (left and middle row) simultaneously with the VLT/CRIRES spectra and spectro-astrometric signal (right row). *Bottom*: Our best-fit kinematical model consists of a Keplerian-rotating disk that emits in Br γ at stellocentric radii from a few stellar radii (< 0.5 AU) to ~ 6.5 AU, while the dust disk starts at 1.8 AU (Kraus et al., 2012b).

1.59 ± 0.25 mas or ~ 1.8 AU (see best-fit model images in Fig. 7, bottom).

Our detection of a Keplerian velocity field provides important evidence for the pre-main-sequence (Herbig B[e]) nature of V921 Sco, as the decretion disks around post-main-sequence supergiant B[e] stars are expected to exhibit a strong outflowing velocity component (Lamers & Pauldrach, 1991), which is not observed in our data. Also, we find that the previous distance estimates have likely underestimated the distance to V921 Sco ($d = 1.15$ kpc), as this distance implies with our measured rotation profile a stellar mass of just $5.4 \pm 0.4 M_{\odot}$, which is significantly lower than expected from the spectral classification.

5 Conclusions

Spectroscopy and interferometry provide highly complementary constraints and extend our observational capabilities in the spectral and spatial domain. We are just starting to explore the scientific opportunities that arise from com-

binning these techniques, but it is clear that the unique combination of high spatial and high spectral resolution could enable transformational studies both in galactic and extragalactic astronomy.

Particularly powerful constraints can be obtained with spectro-interferometry, as I have illustrated with our studies on ζ Tau and V921 Sco, where we constrained the spatial distribution and kinematics of the line-emitting hydrogen gas on scales of a few stellar radii. For faint ($K \lesssim 8$) or strongly resolved objects, it is still rather challenging to perform these observations, mainly due to the stringent requirements on fringe tracking and the low efficiency of filling the uv -plane with 3-telescope interferometric observations. Therefore, we investigated the possibility of combining spectro-interferometry with spectro-astrometric observations that can be conducted with conventional spectrographs, providing a resource-efficient approach to obtain indispensable constraints for a kinematical modeling.

Efficient model-independent imaging should become accessible with the upcoming generation of spectro-interferometric 4-telescope beam combiners and will enable

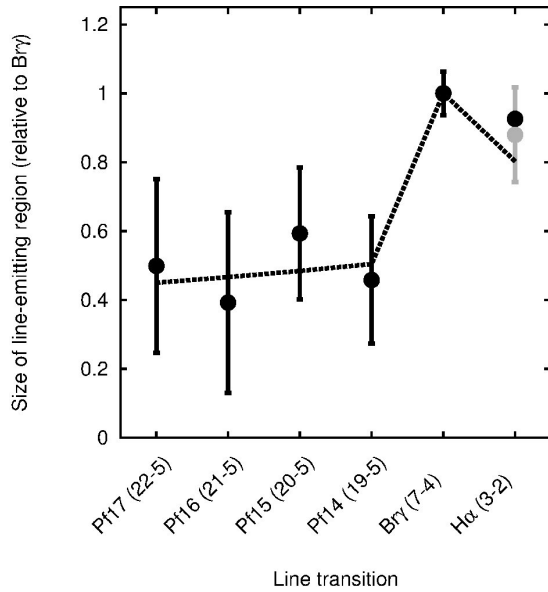


Fig. 5 The size of the line-emitting region in the classical Be star ζ Tau in different line transitions, including four Pfund lines, Br γ , and H α (measurements from Kraus et al. 2012c; Quirrenbach et al. 1994; Vakili et al. 1998 and Tycner et al. 2004). The measured size differences can be reproduced with our simple LTE radiative transfer model (dashed line).

detailed studies on complex velocity structures or on time-variable processes.

References

- Benedettini, M., Nisini, B., Giannini, T., Lorenzetti, D., Tommasi, E., Saraceno, P., & Smith, H. A. 1998, *A&A*, 339, 159
- Borges Fernandes, M., Kraus, M., Lorenz Martins, S., & de Araújo, F. X. 2007, *MNRAS*, 377, 1343
- Brannigan, E., Takami, M., Chrysostomou, A., & Bailey, J. 2006, *MNRAS*, 367, 315
- Caballero, J. A. 2010, *A&A*, 511, L9
- Caballero, J. A., & Solano, E. 2008, *A&A*, 485, 931
- Espaillet, C., Furlan, E., D’Alessio, P., Sargent, B., Nagel, E., Calvet, N., Watson, D. M., & Muzerolle, J. 2011, *ApJ*, 728, 49
- Espaillet, C., et al. 2010, *ApJ*, 717, 441
- Fouchet, L., Gonzalez, J.-F., & Maddison, S. T. 2010, *A&A*, 518, A16
- Kraus, S., Calvet, N., Hartmann, L., Hofmann, K.-H., Kreplin, A., Monnier, J. D., & Weigelt, G. 2012a, *ApJ*, 746, L2
- . 2012b, *ApJ*, 752, 11
- Kraus, S., et al. 2008, *A&A*, 489, 1157
- . 2012c, *ApJ*, 744, 19
- . 2013, *ApJ*, 768, 80
- Lamers, H. J. G., & Pauldrach, A. W. A. 1991, *A&A*, 244, L5

- Millour, F., Meilland, A., Chesneau, O., Stee, P., Kanaan, S., Petrov, R., Mourard, D., & Kraus, S. 2011, *A&A*, 526, A107+
- Mourard, D., et al. 2012, in *Society of Photo-Optical Instrumentation Engineers (SPIE) Conference Series*, Vol. 8445, *Society of Photo-Optical Instrumentation Engineers (SPIE) Conference Series*
- Petrov, R. G. 1989, in *NATO ASIC Proc. 274: Diffraction-Limited Imaging with Very Large Telescopes*, ed. D. M. Alloin & J.-M. Mariotti, 249
- Petrov, R. G., et al. 2007, *A&A*, 464, 1
- Porter, J. M., & Rivinius, T. 2003, *PASP*, 115, 1153
- Quirrenbach, A., Buscher, D. F., Mozurkewich, D., Hummel, C. A., & Armstrong, J. T. 1994, *A&A*, 283, L13
- Schmitt, H. R., et al. 2009, *ApJ*, 691, 984
- Tycner, C., et al. 2004, *AJ*, 127, 1194
- Vakili, F., et al. 1998, *A&A*, 335, 261
- Weigelt, G., et al. 2007, *A&A*, 464, 87